RSC Advances

This is an *Accepted Manuscript*, which has been through the Royal Society of Chemistry peer review process and has been accepted for publication.

Accepted Manuscripts are published online shortly after acceptance, before technical editing, formatting and proof reading. Using this free service, authors can make their results available to the community, in citable form, before we publish the edited article. This *Accepted Manuscript* will be replaced by the edited, formatted and paginated article as soon as this is available.

You can find more information about *Accepted Manuscripts* in the Information for Authors.

Please note that technical editing may introduce minor changes to the text and/or graphics, which may alter content. The journal's standard Terms & Conditions and the Ethical guidelines still apply. In no event shall the Royal Society of Chemistry be held responsible for any errors or omissions in this *Accepted Manuscript* or any consequences arising from the use of any information it contains.

ROYAL SOCIETY OF CHEMISTRY

www.rsc.org/advances

A table of contents entry

Colour graphic

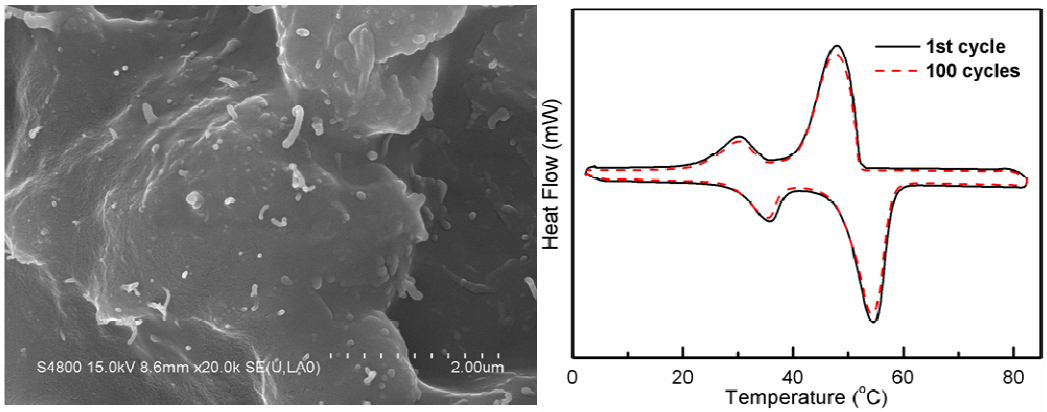

Text

N-octadecylamine-functionalized multi-walled carbon nanotubes (*f*-MWCNTs) are introduced to paraffin to improve thermal conductivity and decrease supercooling of phase change materials.

RSC Advances Accepted Manuscript

RSC Advances

Cite this: DOI: 10.1039/c0xx00000x

ARTICLE TYPE

www.rsc.org/xxxxxx

Improving thermal conductivity and decreasing supercooling of paraffin phase change materials by *n*-octadecylamine-functionalized multi-walled carbon nanotubes

Qianqiu Tang,[† a] Jun Sun,[† a] Shuangmin Yu[a] and Gengchao Wang*[a]

Received (in XXX, XXX) Xth XXXXXXXXX 20XX, Accepted Xth XXXXXXXXX 20XX
DOI: 10.1039/b000000x

Improving thermal conductivity and decreasing supercooling are essential for the utilization of paraffin phase change materials (PCMs). In this work, n-octadecylamine-functionalized multi-walled carbon nanotubes (*f*-MWCNTs) are obtained through a simple method of carboxylation of the MWCNTs with mixed acids of H_2SO_4 and HNO_3 and then salt-forming reaction with n-octadecylamine. The paraffin/*f*-MWCNTs (paraffin/*f*-MWCNTs) composite PCMs are fabricated by mixing paraffin with *f*-MWCNTs under ultrasonication at 70 °C. It is found that the *f*-MWCNTs are homogenously dispersed in toluene or paraffin matrix due to the existence of long chain alkane in *f*-MWCNTs. As a result, the thermal conductivity and heat transfer of the paraffin/*f*-MWCNTs composite PCMs are significantly enhanced. Moreover, differential scanning calorimeter (DSC) analysis indicates that the incorporation of *f*-MWCNTs reduces the supercooling of paraffin, mainly due to the well-dispersed *f*-MWCNTs serving as nuclei to promote the heterogeneous nucleation and crystallization process of paraffin.

1. Introduction

With energy sources becoming intermittent in nature, energy storage and recycling are playing a more important role in conserving available energy and improving its utilization. Due to their great capacity to absorb and slowly release the latent heat involved in phase change process, the phase change materials (PCMs) can be applied in many fields such as solar energy systems, central air-conditioning systems, energy efficient buildings and industrial waste heat recovery, thus attracting great research attention in the recent years[1-7].

Based on the phase-change state, PCMs for latent thermal energy storage fall into three categories: solid-solid, solid-liquid and solid-gas, among which the solid-liquid PCMs are the most suitable for thermal energy storage. The substances used can be organic such as paraffin[8-12], fatty acid and its derivatives[13-20], polyethylene glycol[21-26] and polyalcohols, or inorganic such as salt hydrates[27, 28] and metallic. Compared with inorganic PCMs, the organic ones have received more favor of researchers with less supercooling and noncorrosion to the equipment. One of the most preferred organic PCMs are paraffin waxes because of their favorable thermal-physical properties, such as uniform melting behavior, good stability, easy availability, no toxicity, and no phase segregation during repetitive phase transitions. However, the low thermal conductivity of paraffin (0.3 W/m·K) decreases the overall power of the thermal storage device, which poses a great challenge for their application.

In order to enhance the thermal conductivity of paraffin, great efforts have been attempted by researchers, which mainly includes introducing metal or metal oxide fillers[29-32] and carbon materials [31, 33-37]. Nevertheless, metal or metal oxide fillers add significant weight and cost to the storage systems and some of them are incompatible with paraffin. In comparison, carbon materials, such as carbon nanotubes[38-45], carbon nanofiber[41], graphene[46, 47] and graphite[11, 48-52], which present high thermal conductivity, low bulk density and chemical inertness, are more favorable for modification of PCMs.

With their high thermal conductivity and light weight, carbon nanotubes show tremendous potential as addictives to enhance the thermal condutivity for heat transfer applications. Jifen Wang et al. found that the thermal conductivity of PCMs increased by 40 % with 2 % mass fraction of CNTs. Peijun Ji et al.[43] reported that the latent [42, 53]which restricts the homogenous distribution of CNTs and the practical utilization rate of CNTs as conductive filler. Jifen Wang et al. prepared oleylamine and octanol grafted CNTs to get their more homogenous distribution in palmitic acid and paraffin wax.[42] However, the common methods of modifying CNTs often involve a complicated process of carboxylation, acrylating chlorination and then grafting with organic molecule, which need toxic solvent and vaccum condition.[42, 53-55]

Herein, we report a simple method to modify multi-walled carbon nanotubes (MWCNTs) with *n*-octadecylamine in order to improve the dispersibility of MWCNTs in paraffin wax (shown in Scheme 1). Firstly, the mixed acid of H_2SO_4/HNO_3 was utilized to produce carboxylic groups at the open end of MWCNTs. Then, through salt-forming reaction and hydrogen bonding, *n*-octadecylamine with long aliphatic chain was firmly grafted to the

RSC Advances Accepted Manuscript

surface of MWCNTs so as to produce functionalized carbon nanotubes (*f*-MWCNTs). Finally *f*-MWCNTs and paraffin were homogeneously mixed to get paraffin/*f*-MWCNTs composite PCMs. The influence of the introduction of *f*-MWCNTs on the morphology, structure, thermal conductivity and phase change storage properties of the composite were systematically studied.

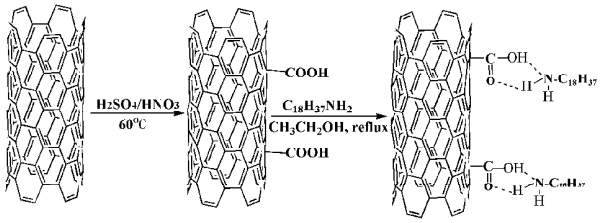

Scheme 1. Schematic illustration of synthesis route for *f*-MWCNTs.

2. Experimental

2.1 Materials

Paraffin with a melting temperature of 52~54 °C was purchased from Aladdin Reagent Co. Ltd. Multiwall carbon nanotubes (MWCNTs) with an average diameter of 10~20 nm were obtained from Chengdu Organic Chemicals Co. Ltd. of Chinese Academy of Sciences. *n*-octadecylamine with a purity of 95% was purchased from Aladdin Reagent Co. Ltd.

2.2 Preparation of *a*-MWCNTs

MWCNTs were purified in 1.5 M chlorhydric acid at 80 °C for 6 h to remove the catalyst particles and other impurities. 4 g of MWCNTs was dispersed in 250 mL mixed acid of H_2SO_4/HNO_3 (v/v 3:1) at 60 °C under constant stirring for 24 h.. The resulting acidic mixture was diluted and washed with deionized water by filtering through a 0.45 μm polyvinylidene fluoride membrane to obtain carboxylated MWCNT (*a*-MWCNT).

2.3 Preparation of *f*-MWCNTs

0.4 g *a*-MWCNTs and 1.0 g *n*-octadecylamine were added into 30 mL ethanol, followed by sonicating for 1 h to obtain well-dispersed suspension. Then the mixed dispersion was refluxed under 78 °C for 24 h. The resulting product was filtered and washed with ethanol for several times. After drying at 60 °C, *n*-octadecylamine functionalized MWCNTs (*f*-MWCNTs) were obtained.

2.4 Preparation of paraffin/*f*-MWCNTs PCM composites

f-MWCNTs with various weight ratio were added to paraffin, and the mixtures were kept at 70°C for 24 h, during which sonication for 1h was undertaken. In this way, a series of *f*-MWCNTs modified paraffin (paraffin/*f*-MWCNTs) composite PCMs were obtained.

2.5 Characterizations

Fourier transform infrared (FTIR) spectra were obtained by a Nicolet 5700 spectrometer with resolution of 2 cm^{-1} using KBr pellets. X-ray diffraction (XRD) patterns were performed in a Rigaku D/Max 2550 VB/PC X-ray diffractometer using Cu (Kα) radiation with the 2θ-angle of 3~50°. The morphologies of the samples were characterized by a field-emission scanning electron microscope (FE-SEM, S4800, Hitachi), and transmission electron microscope (TEM, JEM-1400, JEOL) and high resolution transmission electron microscopy (HRTEM, JEOL JEM-2100). X-ray photoelectron spectroscopy (XPS) was recorded with a thermo scientific ESCALAB 250Xi X-ray photoelectron spectrometer equipped with a monochromatic Al Kα X-ray source (1486.6 eV). Photographs showing the dispersion stability in toluene were recorded using a digital camera (FinePix-F420, Fuji). The dispersion stability of the samples was studied using an analyzer of concentrated liquid dispersion from Formulaction Corporation. The aqueous suspension of the samples was contained in a cylindrical glass cell. The light source was an electro luminescent diode in the near infrared (λ=880nm). Thermal properties were measured on a differential scanning calorimetric instrument (modulated DSC2910, TA) running from 0 to 80 °C at a heating rate of 5 °C/min under nitrogen. The thermal conductivity of the samples was measured with a Hot Disk Thermal Constant Analysers TPS 2500. The heat storage (release) curves were tested as following procedure: The samples of paraffin and the composite PCMs with the same volume were melted by heating, and then they were put into glass tubes with 20 mm inner diameter. Temperature probe was inserted to the center of the PCMs materials, and when the temperature stabilized at 30 °C, the glass tubes were transferred to a 70 °C thermostatic waterbath. Finally, the heat storage curves were recorded by a computer controlled data acquisition system with an interval data recordation time of 3 s. To obtain the heat release curves, the glass tubes with PCMs were put into a 70 °C thermostatic waterbath, and when the temperature stabilized at 70 °C, the glass tubes were transferred to air environment of 20 °C.

3. Results and discussion

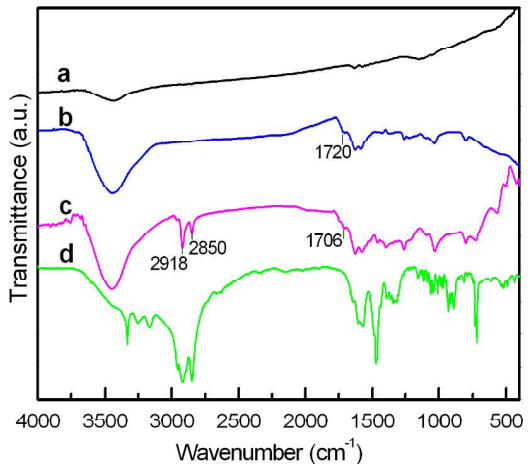

Fig. 1. FTIR spectra of (a) crude MWCNTs, (b) *a*-MWCNTs, (c) *f*-MWCNTs, and (d) *n*-octadecylamine.

Fig. 1 shows the FTIR spectra of crude MWCNTs, *a*-MWCNTs, *f*-MWCNTs and *n*-octadecylamine. For the spectrum of *a*-MWCNTs (Fig.1b), the band at 1720 cm^{-1} is assigned to the C=O stretching vibration, indicating the introduction of carboxyl groups after the mixture acid treatment. Besides, compared with crude MWCNTs, the O-H peak at 3400 cm^{-1} is strengthened. In the spectrum of *f*-MWCNTs, the prominent peaks at 2918 and

RSC Advances Accepted Manuscript

This journal is © The Royal Society of Chemistry [year]

2850 cm^{-1} are assigned to the CH_3- and -CH_2- bond vibration, while the stretching vibration of N-H in the range of 3100~3350 cm^{-1} does not appear (Fig.1c). It indicates that the amino groups in *n*-octadecylamine react with the carboxyl groups of *a*-MWCNTs, and the *n*-octadecylamine is grafted onto *a*-MWCNTs. Fig.1 also shows that the prominent C=O peak of *f*-WMCNTs red shifts from 1720 cm^{-1} to 1706 cm^{-1}, which is ascribed to the formation of hydrogen bond between the C=O and N-H groups. Furthermore, the XPS spectrum (Fig. S1) also indicates the existence of N elements in *f*-WMCNTs, confirming the successfully functionalization by *n*-octadecylamine.

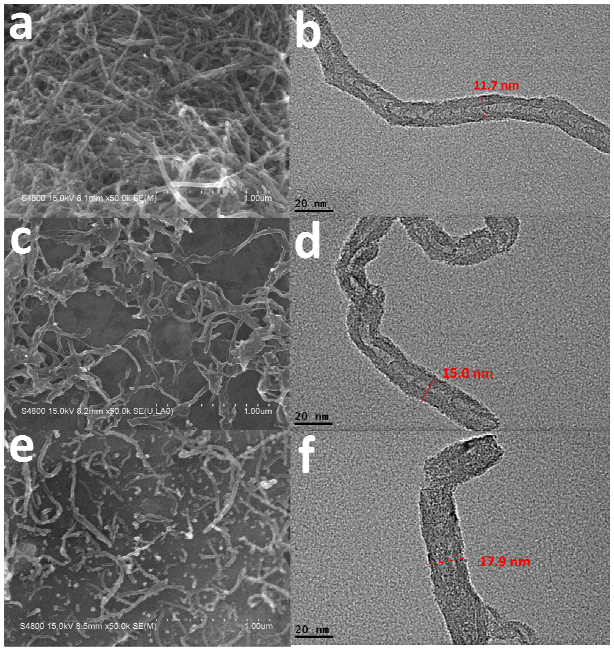

Fig. 2. FESEM images of (a) crude MWCNTs, (c) *a*-MWCNTs, and (e) *f*-MWCNTs. (scale bars: 1 μm). HRTEM images of (b) crude MWCNTs, (d) *a*-MWCNTs, and (f) *f*-MWCNTs in toluene.

Fig. 2 shows the FESEM and HRTEM images of MWCNTs, *a*-MWCNTs, and *f*-MWCNTs. It can be seen from Fig. 2a and 2b that the crude MWCNTs present a state of mutual entanglement with a diameter of 11.7 nm. The crude MWCNTs also exhibit bad dispersibility in toluene (Fig. S2a). In comparison, the *a*-MWCNTs (Fig. 2c) are cut short, and show better dispersibility with no obvious entanglement in toluene (Fig. S2b) compared with crude MWCNTs. Besides, its surface shows some defects due to acid mixture treatment (Fig. 2d). After being functionalized with *n*-octadecylamine, *f*-MWCNTs (Fig. 2e and 2f) exhibit a bigger average diameter of 17.9 nm and more obscure surface than *a*-MWCNTs as well as better dispersibility (Fig. S2c). It is due to the fact that *n*-octadecylamine is successfully grafted onto the surface of *a*-MWCNTs.

Fig. 3 presents the digital photos of the dispersion stability of MWCNTs and *f*-MWCNTs in toluene. The crude MWCNTs completely precipitate after 1 h (Fig. 3a). In comparison, *f*-MWCNTs show no precipitation after sedimentation for 48 h (Fig. 3b), indicating the significant improved dispersion stability of *f*-MWCNTs in toluene. It can be explained as follows. The *n*-octadecylamine with long chain alkane is grafted onto *f*-MWCNTs, which results in the good compatibility between *f*-MWCNTs and toluene solvent according to the theory of "similarity and intermiscibility".

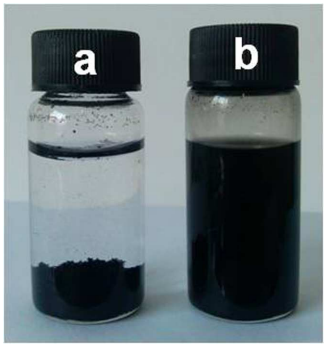

Fig. 3. Digital photos showing dispersion stability in toluene of (a) crude MWCNTs for 1h and (b) *f*-MWCNTs for 48 h.

To further evaluate the dispersion stability of MWCNTs and *f*-MWCNTs in toluene, an analyzer of concentrated liquid dispersion from Formulaction Corporation is employed. Fig. 4 gives the backscattering percentage versus sediment time for crude MWCNTs and *f*-MWCNTs in toluene. The backscattering percentage increases with increasing average size of suspended particles. Therefore, we can determine the size change of particles through the change of the backscattering percentage. It is found that the backscattering percentage of crude MWCNTs changes rapidly from 1.99 % to 11.7 % just after 1 h, indicating the quite poor dispersion stability of crude MWCNTs in toluene (Fig. 4a). In comparison, for the *f*-MWCNTs, the change of backscattering percentage is slight after sedimentation for 115 h (Fig. 4b), which is in good accordance with the result of digital photographs (Fig. 3). This further proves that the *f*-MWCNTs have excellent dispersion stability in toluene.

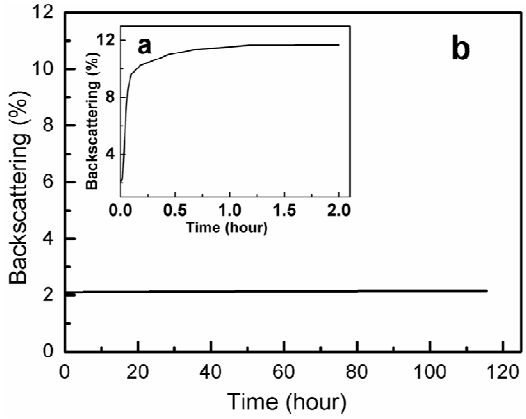

Fig. 4. The backscattering percentage versus sediment time in toluene for (a) crude MWCNTs and (b) *f*-MWCNTs.

The FESEM images of paraffin/crude MWCNTs and paraffin/*f*-MWCNTs composites PCMs with different *f*-MWCNTs contents are shown in Fig. 5. It is obvious that the crude MWCNTs show mutual entanglement (pointed with blue square in Fig. 5a) in paraffin. Besides, they exhibit bad dispersibility with part of the paraffin matrix without the distribution of MWCNTs. For all the paraffin/*f*-MWCNTs composite PCMs, the *f*-MWCNTs are uniformly distributed in the paraffin matrix (pointed with red circles), indicating that the *f*-

RSC Advances Accepted Manuscript

MWCNTs have better compatibility with the paraffin matrix after the *n*-octadecylamine modification. In this case, *f*-MWCNTs can form mutual interpenetrating network structure in the composite system, which is advantageous for the improvement of thermal conductivity.

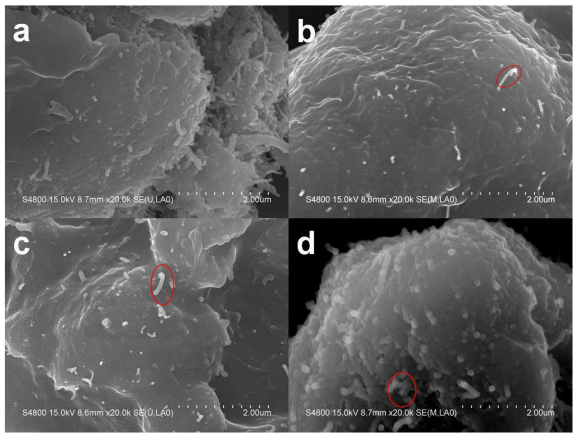

Fig. 5. FESEM images of (a) paraffin/crude MWCNTs (95/5) and paraffin/*f*-MWCNTs composite PCMs with different *f*-MWCNTs contents: (b) 1 wt%, (c) 5 wt%, (d) 10 wt%.

Table 1 DSC test data of paraffin, paraffin/crude MWCNTs and paraffin/f-MWCNTs composite PCMs

Samples	T_f (°C)	T_m (°C)	ΔT(°C)	ΔH_f (J/g)	ΔH_m (J/g)
paraffin	47.2	55.7	8.5	124.4	127.8
paraffin/crude MWCNT (95/5)	47.9	55.2	7.3	129.7	129.3
paraffin/*f*-MWCNTs (99/1)	48.4	54.6	6.2	138.8	138.6
paraffin/*f*-MWCNTs (95/5)	48.0	54.7	6.7	139.3	140.1
paraffin/*f*-MWCNTs (90/10)	48.2	54.6	6.4	119.6	122.1

Fig. 6 shows the DSC heating and cooling curves of the paraffin, paraffin/crude MWCNTs and paraffin/*f*-MWCNTs composite PCMs with different *f*-MWCNTs contents at a scanning rate of 5 °C/min. It can be observed that pure paraffin and their composite PCMs all exhibit two characteristic peaks. The relatively weak peak at lower temperature range corresponds to the solid-to-solid state transfer, and the main peak at higher temperature range is attributed to the solid-liquid state transfer (the melting temperature T_m or crystallization temperature T_f)[39, 56]. Thus, it can be inferred that the introduction of *f*-MWCNTs does not change the main structure of paraffin matrix. The difference between T_m and T_f is defined as the supercooling temperature (ΔT), and a smaller ΔT is more advantageous for phase change energy storage. From Table 1, it can be observed that the melting/crystallization peak temperature of pure paraffin is 55.7 and 47.2 °C, so the supercooling temperature is 8.5 °C. With the addition of 1, 5 and 10 wt% *f*-MWCNTs, the supercooling temperature of the composite PCMs decreases to 6.2, 6.7 and 6.4 °C, respectively. Thus the introduction of *f*-MWCNTs suppresses the supercooling to some extent, and the main reasons can be explained by *f*-MWCNTs functioning as nucleation agent. Without adding foreign additives, the crystallization process of pure paraffin is sluggish, leading to a larger supercooling. The well dispersed *f*-MWCNTs provide stable foreign nuclei to promote the heterogeneous nucleation and accelerate crystallization process.

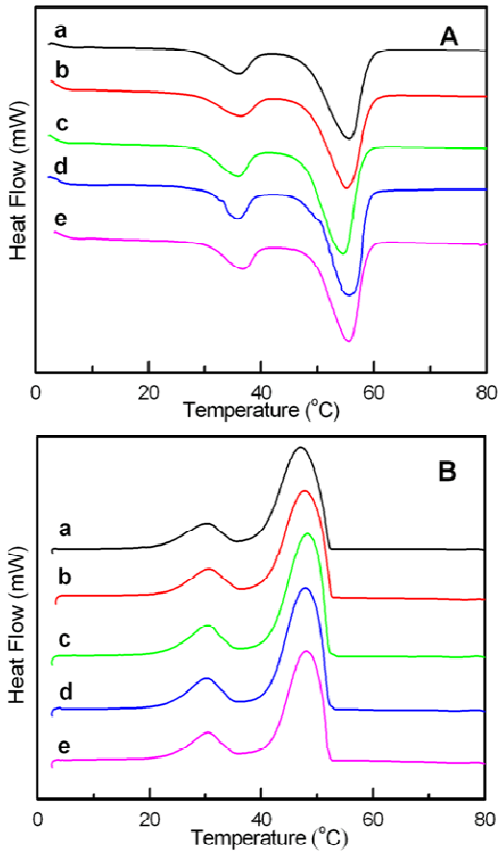

Fig. 6. DSC (A) heating curves and (B) cooling curves for (a) paraffin, (b) paraffin/crude MWCNTs (95/5) and paraffin/*f*-MWCNTs composite PCMs with different *f*-MWCNTs contents: (c) 1wt %, (d) 5 wt%, (e) 10 wt%.

From the Table 1, it is noticed that the latent heat capacity of pure paraffin is 124.4 J/g, while the latent capacities of the composite PCMs with 1.0 and 5.0 wt% *f*-MWCNTs increase to 138.8 and 139.3 J/g, respectively. The enhancement of the latent capacities of the composites can be explained by *f*-MWCNTs functioning as heterogeneous nucleation agent, which is advantageous for the crystallization growth of paraffin. When further increasing the amount of *f*-MWCNTs to 10 wt%, the latent capacities decrease to 119.6 J/g. It is ascribed that too much *f*-MWCNTs restrain the crystallization growth of paraffin and reduce the ratio of phase change component paraffin in the composite.

Furthermore, the composite with the addition of 5 wt% *f*-MWCNTs has smaller supercooling effect and higher latent capacity than that with 5 wt% crude MWCNTs. With the same amount of carbon nanotubes added, the better dispersibility of *f*-MWCNTs can form more homogenous nucleation site than crude MWCNTs, which is more advantageous for the heterogeneous nucleation and crystallization growth of paraffin

RSC Advances Accepted Manuscript

This journal is © The Royal Society of Chemistry [year]

matrix. Thus, compared with paraffin/crude MWCNTs, paraffin/*f*-MWCNTs has smaller supercooling effect and higher latent capacity.

To further evaluate the effect of *f*-MWCNTs on the crystallization properties of paraffin, X-ray diffraction analysis is performed. Fig. 7 shows the XRD patterns of paraffin and paraffin/*f*-MWCNTs composite PCMs with different *f*-MWCNTs contents. The obvious diffraction peaks at 21.5 and 23.8° can be observed for all the samples, corresponding to [110] and [200] of paraffin, respectively. The peak position of the composite PCMs does not shift compared with pure paraffin, indicating that *f*-MWCNTs do not change the crystal structure of paraffin.

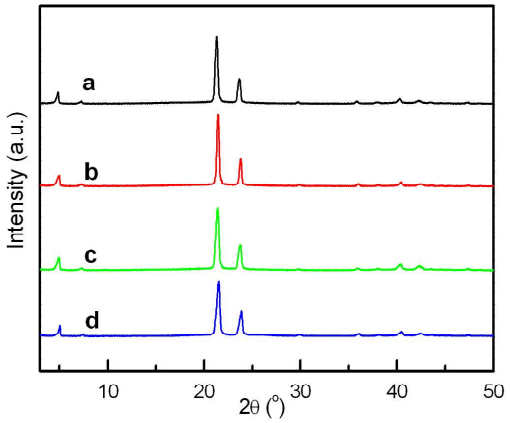

Fig. 7. XRD patterns of (a) paraffin and paraffin/*f*-MWCNTs composite PCMs with different *f*-MWCNTs contents: (b) 1 wt%, (c) 5 wt%, (d) 10 wt %.

Besides, the peak at 21.5° and 23.8° for pure paraffin has a peak intensity ratio (I_{110}/I_{200}) of 2.55. In comparison, with the addition of 1 wt% *f*-MWCNTs, the composite PCMs exhibit a slightly higher I_{110}/I_{200} of 2.57, indicating that relatively small amount of *f*-MWCNTs have positive inductive effect for the crystallization of paraffin. When further increasing the amount of *f*-MWCNTs to 5 wt% and 10 wt%, I_{110}/I_{200} decrease to 2.42 and 2.16, respectively. This indicates that too much *f*-MWCNTs have bad effect on the normal arrangement of paraffin molecular, resulting in the change of intensity of diffraction peaks.

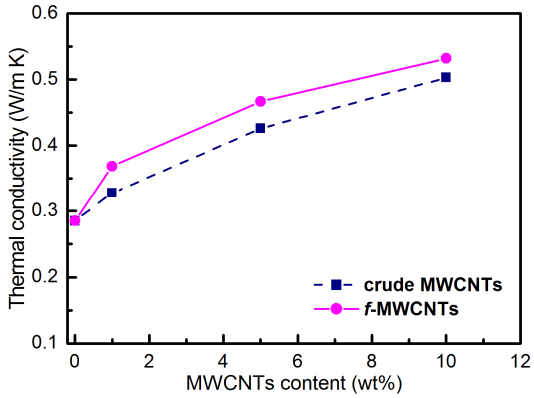

Fig. 8. Influence of crude MWCNTs and *f*-MWCNTs content on thermal conductivity of paraffin/*f*-MWCNTs composite PCMs.

PCMs are used for the thermal storage device. One of the key performance parameters is the rates of heat storage and release, which highly rely on the thermal conductivity of the PCMs. Fig. 8 reflects the influence of the *f*-MWCNTs amount on the thermal conductivity of the paraffin/*f*-MWCNTs composite PCMs. For pure paraffin, the thermal conductivity is 0.285 W/m·K. When introducing 1, 5, 10 wt% *f*-MWCNTs to paraffin, the thermal conductivity increases to 0.369, 0.467 and 0.532 W/m·K, respectively. Thus, it can be concluded that the introduction of f-MWCNTs significantly enhances the thermal conductivity of the composites. Besides, comparing the influence of crude MWCNTs and *f*-MWCNTs, it is obvious that *f*-MWCNTs show a more positive effect on the thermal conductivity, which is attributed to better dispersibility of *f*-MWCNTs and utilization rate in the composite PCMs.

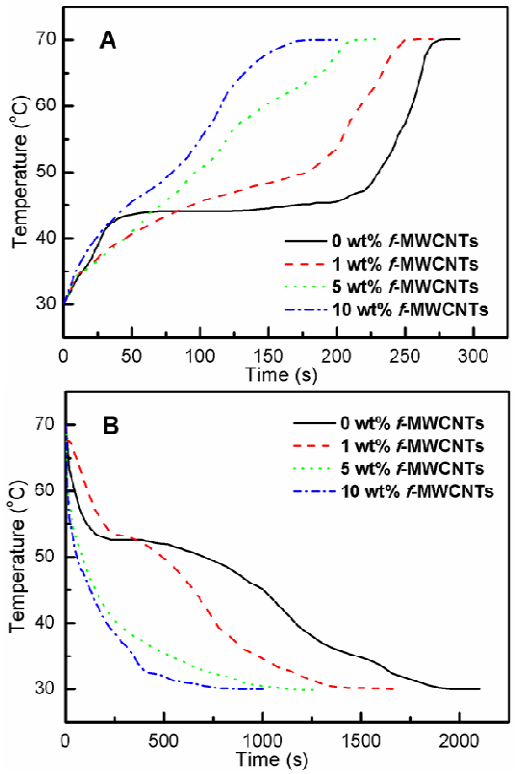

Fig. 9. (A) Heat storage curves and (B) Heat release curves of paraffin and paraffin/*f*-MWCNTs composite PCMs.

Fig. 9 shows the heat storage and heat release curves of paraffin and paraffin/f-MWCNTs composite PCMs. As can be seen from the heat storage curve, it takes 280 s for paraffin to increase the equilibrium temperature from 30°C to 70 °C. Besides, the temperature rises rather slow with quite a long heat storage platform at *ca* 45 °C. When adding 1, 5, 10 wt% *f*-MWCNTs, the time taken for the temperature from 30 °C to 70 °C is reduced to 250, 210, and 180 s, showing improved heat transfer rate of the composites. From the heat release curves, the pure paraffin takes 1960 s to drop from 70 °C to 30 °C, whereas only 960-1600 s is taken for the composite PCMs. This is attributed to the fact that the addition of *f*-MWCNTs improves the thermal conductivity of the composite PCMs, facilitating the heat transfer in the heat storage (release) process. Thus, the heat storage and release time

RSC Advances Accepted Manuscript

to get equilibrium temperature is reduced for paraffin/*f*-MWCNTs composite PCMs.

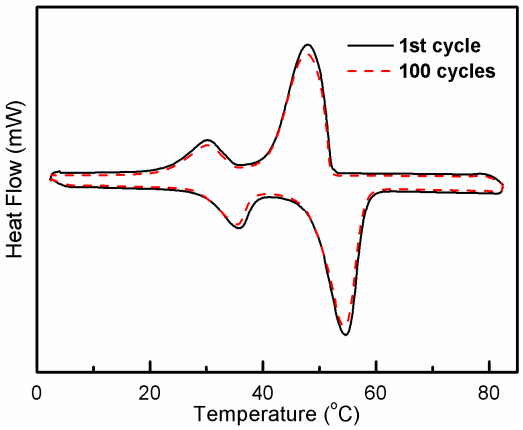

Fig. 10. The DSC curves of paraffin/*f*-MWCNTs (95/5) composite PCM for the first cycle and after 100 cycles.

To evaluate the cycling stability of the composite PCMs, the DSC curves of paraffin/*f*-MWCNTs (95/5) in the first heating-cooling cycle and after 100 cycles are shown in Fig. 10. As can be seen, the two curves almost overlap with each other and exhibit good symmetry. The melting temperature in the first cycle is 54.7 °C, and after 100 cycles, the composite shows rather close T_m of 54.5 °C. Besides, the supercooling temperature (6.8 °C) after 100 cycles is almost unchanged compared with the first cycle (6.7 °C). These results indicate that *f*-MWCNTs shows rather good dispersion stability with no significant precipitation and aggregation during heating-cooling cycles. What's more, the latent capacity of the composite slowly decreases from 139.3 J/g to 128.7 J/g after 100 cycles, further confirming the good cycling stability of the paraffin/*f*-MWCNTs composite PCMs.

4. Conclusions

The functionalized multi-walled carbon nanotubes grafted with *n*-octadecylamine (*f*-MWCNTs) are utilized to improve the dispersibility of MWCNTs in paraffin. Compared with crude MWCNTs, *f*-MWCNTs exhibit enhanced thermal conductivity and reduced supercooling, which are attributed to the good compatibility between paraffin and the long chain alkane in *f*-MWCNTs as well as *f*-MWCNTs serving as crystallization nuclei. The thermal conductivity of the paraffin/*f*-MWCNTs composite PCMs increases with increasing *f*-MWCNTs content. With 10 wt% *f*-MWCNTs, the thermal conductivity of composite PCMs increases by 86.7 %. It is also encouraging that the *f*-MWCNTs have significant effect in reducing supercooling. With 1 wt% *f*-MWCNTs, the supercooling temperature decreases by 27 %. Moreover, the paraffin/*f*-MWCNTs composite PCMs also show excellent thermal cycling stability.

Acknowledgements

This work was supported by National Natural Science Foundation of China (51173042), Shanghai Municipal Science and Technology Commission (12nm0504102), and Fundamental Research Funds for the Central Universities.

Notes and references

† *These authors contributed equally to this work.*

[a] *Shanghai Key Laboratory of Advanced Polymeric Materials, Key Laboratory for Ultrafine Materials of Ministry of Education, School of Materials Science and Engineering, East China University of Science and Technology, Shanghai 200237, China. E-mail: gengchaow@ecust.edu.cn*

1 F. Agyenim, N. Hewitt, P. Eames and M. Smyth, *Renew Sust Energ Rev*, 2010, **14**(2), 615.

2 B. M. Diaconu, S. Varga and A. C. Oliveira, *Appl Energy*, 2010, **87**(2), 620.

3 R. Baetens, B. P. Jelle and A. Gustavsen, *Energy Build*, 2010, **42**(9), 1361.

4 V. V. Tyagi, S. C. Kaushik, S. K. Tyagi and T. Akiyama, *Renew Sust Energ Rev*, 2011, **15**(2), 1373.

5 W. Hu and X. Yu, *Rsc Advances*, 2012, **2**(13), 5580.

6 Y. Wang, B. Tang and S. Zhang, *Journal Of Materials Chemistry*, 2012, **22**(35), 18145.

7 M. Upadhyay, S. Abhaya, S. Murugavel and G. Amarendra, *Rsc Advances*, 2014, **4**(8), 3691.

8 T. Kousksou, A. Jamil, T. El Rhafiki and Y. Zeraouli, *Solar Energy Materials and Solar Cells*, 2010, **94**(12), 2158.

9 O. Sanusi, R. Warzoha and A. S. Fleischer, *International Journal of Heat and Mass Transfer*, 2011, **54**(19-20), 4429.

10 M. Li, Z. S. Wu, H. T. Kao and J. M. Tan, *Energy Conv Manag*, 2011, **52**(11), 3275.

11 Z. G. Zhang, N. Zhang, J. Peng, X. M. Fang, X. N. Gao and Y. T. Fang, *Appl Energy*, 2012, **91**(1), 426.

12 Y. Qian, P. Wei, P. K. Jiang and J. P. Liu, *Solar Energy Materials and Solar Cells*, 2012, **107**, 13.

13 L. J. Wang and D. Meng, *Appl Energy*, 2010, **87**(8), 2660.

14 A. Sari, A. Bicer, A. Karaipekli, C. Alkan and A. Karadag, *Solar Energy Materials and Solar Cells*, 2010, **94**(10), 1711.

15 M. Li, H. T. Kao, Z. S. Wu and J. M. Tan, *Appl Energy*, 2011, **88**(5), 1606.

16 M. Li, Z. S. Wu and H. T. Kao, *Appl Energy*, 2011, **88**(9), 3125.

17 A. A. Aydin and H. Okutan, *Solar Energy Materials and Solar Cells*, 2011, **95**(10), 2752.

18 A. Sari and A. Bicer, *Solar Energy Materials and Solar Cells*, 2012, **101**, 114.

19 A. A. Aydin, *Solar Energy Materials and Solar Cells*, 2013, **113**, 44.

20 W. D. Liang, G. D. Zhang, H. X. Sun, Z. Q. Zhu and A. Li, *Rsc Advances*, 2013, **3**(39), 18022.

21 Y. Fang, H. Y. Kang, W. L. Wang, H. Liu and X. N. Gao, *Energy Conv Manag*, 2010, **51**(12), 2757.

22 L. L. Feng, W. Zhao, J. Zheng, S. Frisco, P. Song and X. G. Li, *Solar Energy Materials and Solar Cells*, 2011, **95**(12), 3550.

23 B. T. Tang, M. G. Qiu and S. G. Zhang, *Solar Energy Materials and Solar Cells*, 2012, **105**, 242.

24 Y. M. Wang, B. T. Tang and S. F. Zhang, *Rsc Advances*, 2012, **2**(30), 11372.

25 J. R. Li, L. H. He, T. Z. Liu, X. J. Cao and H. Z. Zhu, *Solar Energy Materials and Solar Cells*, 2013, **118**, 48.

26 B. Tang, Y. Wang, M. Qiu and S. Zhang, *Solar Energy Materials and Solar Cells*, 2014, **123**, 7.

27 C. Y. Zhao and Z. G. Wu, *Solar Energy Materials and Solar Cells*, 2011, **95**(12), 3341.

RSC Advances Accepted Manuscript

This journal is © The Royal Society of Chemistry [year]

28 P. Hu, D. J. Lu, X. Y. Fan, X. Zhou and Z. S. Chen, *Solar Energy Materials and Solar Cells*, 2011, **95**(9), 2645.
29 S. Y. Wu, D. S. Zhu, X. R. Zhang and J. Huang, *Energy & Fuels*, 2010, **24**, 1894.
30 G. L. Song, S. D. Ma, G. Y. Tang, Z. S. Yin and X. W. Wang, *Energy*, 2010, **35**(5), 2179.
31 C. Y. Zhao and Z. G. Wu, *Solar Energy Materials and Solar Cells*, 2011, **95**(2), 636.
32 J. L. Zeng, F. R. Zhu, S. B. Yu, L. Zhu, Z. Cao, L. X. Sun, G. R. Deng, W. P. Yan and L. Zhang, *Solar Energy Materials and Solar Cells*, 2012, **105**, 174.
33 L. W. Fan and J. M. Khodadadi, *Renew Sust Energ Rev*, 2011, **15**(1), 24.
34 L. L. Feng, J. Zheng, H. Z. Yang, Y. L. Guo, W. Li and X. G. Li, *Solar Energy Materials and Solar Cells*, 2011, **95**(2), 644.
35 P. M. Gilart, A. Y. Martinez, M. G. Barriuso and C. M. Martinez, *Solar Energy Materials and Solar Cells*, 2012, **107**, 205.
36 C. Y. Wang, L. L. Feng, W. Li, J. Zheng, W. H. Tian and X. G. Li, *Solar Energy Materials and Solar Cells*, 2012, **105**, 21.
37 X. Xiao and P. Zhang, *Solar Energy Materials and Solar Cells*, 2013, **117**, 451.
38 J. Wang, H. Xie and Z. Xin, *Journal of Applied Physics*, 2008, **104**(11), 113537.
39 J. F. Wang, H. Q. Xie, Z. Xin, Y. Li and L. F. Chen, *Solar Energy*, 2010, **84**(2), 339.
40 S. Shaikh and K. Lafdi, *Carbon*, 2010, **48**(3), 813.
41 Y. B. Cui, C. H. Liu, S. Hu and X. Yu, *Solar Energy Materials and Solar Cells*, 2011, **95**(4), 1208.
42 J. Wang, H. Xie and Z. Xin, *Journal of Materials Science & Technology*, 2011, **27**(3), 233.
43 P. J. Ji, H. H. Sun, Y. X. Zhong and W. Feng, *Chem Eng Sci*, 2012, **81**, 140.
44 X. Meng, H. Zhang, L. Sun, F. Xu, Q. Jiao, Z. Zhao, J. Zhang, H. Zhou, Y. Sawada and Y. Liu, *Journal of Thermal Analysis and Calorimetry*, 2012, **111**(1), 377.
45 Y. Wang, B. Tang and S. Zhang, *Advanced Functional Materials*, 2013, **23**(35), 4354.
46 F. Yavari, H. R. Fard, K. Pashayi, M. A. Rafiee, A. Zamiri, Z. Z. Yu, R. Ozisik, T. Borca-Tasciuc and N. Koratkar, *Journal of Physical Chemistry C*, 2011, **115**(17), 8753.
47 Y. J. Zhong, M. Zhou, F. Q. Huang, T. Q. Lin and D. Y. Wan, *Solar Energy Materials and Solar Cells*, 2013, **113**, 195.
48 P. Zhang, Y. Hu, L. Song, J. X. Ni, W. Y. Xing and J. Wang, *Solar Energy Materials and Solar Cells*, 2010, **94**(2), 360.
49 L. Xia, P. Zhang and R. Z. Wang, *Carbon*, 2010, **48**(9), 2538.
50 J. L. Xiang and L. T. Drzal, *Solar Energy Materials and Solar Cells*, 2011, **95**(7), 1811.
51 L. Xia and P. Zhang, *Solar Energy Materials and Solar Cells*, 2011, **95**(8), 2246.
52 S. G. Jeong, O. Chung, S. Yu and S. Kim, *Solar Energy Materials and Solar Cells*, 2013, **117**, 87.
53 S. S. Kish, A. Rashidi, H. R. Aghabozorg and L. Moradi, *Applied Surface Science*, 2010, **256**(11), 3472.
54 G. X. Chen and H. Shimizu, *Polymer*, 2008, **49**(4), 943.
55 C. Desai, S. A. Ntim and S. Mitra, *Journal of Colloid and Interface Science*, 2012, **368**, 115.
56 Y. B. Cai, Y. Hu, L. Song, Y. Tang, R. Yang, Y. P. Zhang, Z. Y. Chen and W. C. Fan, *J Appl Polym Sci*, 2006, **99**(4), 1320.

RSC Advances Accepted Manuscript